Our reference: JJBE3072

AUTHOR QUERY FORM

ELSEVIER	**Journal: JJBE** **Article Number: 3072**	**Please e-mail your responses and anycorrections to:** **E-mail: correctionsaptara@elsevier.com**

Dear Author,

Please check your proof carefully and mark all corrections at the appropriate place in the proof (e.g., by using on-screen annotation in the PDF file) or compile them in a separate list. Note: if you opt to annotate the file with software other than Adobe Reader then please also highlight the appropriate place in the PDF file. To ensure fast publication of your paper please return your corrections within 48 hours.

Your article is registered as belonging to the Special Issue/Collection entitled "MNF2016". If this is NOT correct and your article is a regular item or belongs to a different Special Issue please contact r.eyles@elsevier.com immediately prior to returning your corrections.

For correction or revision of any artwork, please consult http://www.elsevier.com/artworkinstructions

Any queries or remarks that have arisen during the processing of your manuscript are listed below and highlighted by flags in the proof. Click on the '**Q**' link to go to the location in the proof.

Location in article	**Query / Remark: click on the Q link to go** **Please insert your reply or correction at the corresponding line in the proof**
Q1	AU: The author names have been tagged as given names and surnames (surnames are highlighted in teal color). Please confirm if they have been identified correctly.
Q2	AU: Please provide complete affiliation details.
Q3	AU: Figs. 2, 3, 4, 5 have been submitted as color images; however, the captions have been reworded to ensure that they are meaningful when your article is reproduced both in color and in black and white. Please check and correct if necessary.
Q4	AU: Please provide the grant number for the grant sponsor provided and validate the grant sponsors for correctness.
	Please check this box or indicate your approval if you have no corrections to make to the PDF file ☐

Thank you for your assistance.

Highlights

• The width of a fluid jet in a rectangular microchannel follows a universal power law. • Microcapsules can be sorted by size at low flow strength. • Microcapsules can be sorted by deformability at high flow strength.

Medical Engineering and Physics xxx (2017) xxx–xxx

Contents lists available at ScienceDirect

Medical Engineering and Physics

journal homepage: www.elsevier.com/locate/medengphy

Deformability- and size-based microcapsule sorting

Q1 Doriane Vesperini[a], Oriane Chaput[a], Nadège Munier[a], Pauline Maire[a], Florence Edwards-levy[b], Anne-Virginie Salsac[a], Anne Le goff[a,*]

Q2 [a] Biomécanique et Bioingénierie (UMR CNRS 7338), Université de Technologie de Compiègne - Sorbonne Universités, France
[b] Institut de Chimie Moléculaire de Reims (UMR CNRS 7312), Faculté de Pharmacie, Université de Reims Champagne-Ardenne, France

ARTICLE INFO

Article history:
Received 19 January 2017
Revised 20 June 2017
Accepted 25 June 2017
Available online xxx

MSC:
00-01
99-00

Keywords:
Microfluidics
Capsule
Deformability
Separation

ABSTRACT

Biomedical applications often require to sort cells according to their physical properties, such as size, density or deformability. In recent years, microfluidics has provided a variety of tools to sort micro-objects. We present here a simple microfluidic device consisting of a channel containing a semi-cylindrical obstacle against which capsules are squeezed by the flow, followed by a diverging chamber where streamlines separate. We demonstrate that this basic system is capable of sorting elastic microcapsules according to their size at low flow strength, and according to the stiffness of their membrane at high flow strength. While most existing devices exhibit their best performances when the size or deformability contrast is maximal, we show that our device is capable of discriminating between capsules whose membrane elasticity differs by a factor of order unity.

1. Introduction

The shape and mechanical properties of blood cells govern many important phenomena, such as margination [1], adhesion [2], and extravasation [3]. Pathologies such as cancer [4] or infections [5] may alter cell size and stiffness. Abnormal stiffness can be used as a sorting parameter in the detection and isolation of pathological cells [6].

Microfluidics presents many advantages for cancer diagnosis applications, such as small reaction volumes, high sensitivity, and ability to sort micro-objects (particles, capsules, and cells) as described in [7]. Among label-free separation techniques, the most studied are size-based sorting devices: deterministic lateral displacement [8,9] , dielectrophoresis [10] , hydrophoresis [11] , acoustic waves [12,13] , and inertia [14]. Other methods based on chemical properties sort micro-objects thanks to the composition of their membrane, such as immunocapture [15] and fluorescence-activated sorting [16]. Finally, other techniques such as optical stretchers [17] and stiffness-dependent separation [18] can sort heterogeneous populations based on their mechanical properties. While size-based microfluidic sorting has already been studied extensively [19], the concept of sorting based on deformability has emerged more recently and proves very promising [18,20].

In bioengineering, particles, capsules and vesicles are considered as simplified models for cells [21–23]. Capsules are biomimetic micro-objects consisting of a thin elastic membrane reticulated around a liquid core. The membrane can be made of natural components such as proteins: human serum albumin (HSA) [24], or ovalbumin [25]. The behavior of capsules is studied under conditions mimicking physiological situations, such as flowing through a constriction [26], and in the context of drug encapsulation and delivery [27].

The influence of confinement has been extensively studied for millimetric and micrometric capsules flowing through cylindrical [25], square [28], or rectangular channels [29].

In a recent numerical study, Zhu et al. [30] proposed to sort elastic capsules based on their deformability by flowing them around an obstacle through a straight channel followed by a diverging chamber. The experimental validation of deformability-based sorting techniques is not trivial because of the lack of homogeneous populations of micro-objects with well-controlled stiffness. We have created a microfluidic device with such a geometry. We use spherical albumin microcapsules whose mechanical properties depend on the production conditions.

In this article, we evaluate the feasibility of experimentally sorting heterogeneous populations of microcapsules depending on their stiffness.

* Corresponding author.
E-mail address: anne.le-goff@utc.fr (A.-V. Salsac).

http://dx.doi.org/10.1016/j.medengphy.2017.06.040
1350-4533/

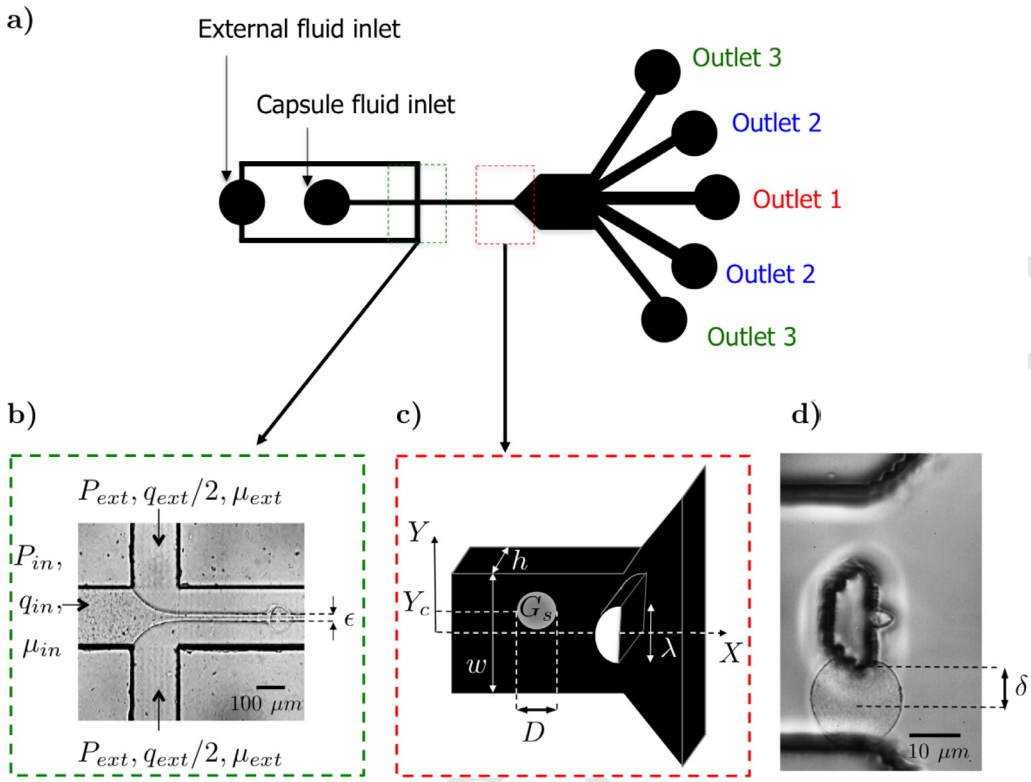

Fig. 1. Sketch of the experimental device. The fluids flow from left to right. (a) General view of our sorting device. (b) Photograph of the flow-focusing at the entrance of the straight channel. The capsule suspension is pinched by an external viscous fluid of viscosity μ_{ext}, and forms a fluid thread of viscosity μ_{in} and thickness ϵ. (c) Dimensions of the obstacle and of the rectangular straight channel. (d) The distance between the center of mass of the capsule and the obstacle is defined as δ.

2. Materials and methods

2.1. Capsule suspensions

Capsules are prepared by interfacial cross-linking as described elsewhere [31]. Briefly, a water-in-oil emulsion is formed using a 10% ovalbumin solution in a phosphate buffer pH 5.9 or pH 8, dispersed in cyclohexane added with 2% m/V sorbitan trioleate. Adding 2.5% (w/v) terephtaloyl chloride to the organic phase induces ovalbumin cross-linking at the interface and the formation of the membrane. This chemical reaction is stopped by dilution with chloroform:cyclohexane (1:4, v/v) after 5 min. Capsules are then rinsed with an aqueous solution of polysorbate, then with pure water, resuspended in water and stored at 4 °C. We obtain a polydisperse population of capsules of diameter D, determined with the Image J software using a circular fit, and expressed as the mean ± the standard deviation. The deformability of capsules obtained by this protocol has been shown to depend on the pH of the buffer solution containing ovalbumin. Capsules prepared at higher pH are more rigid than those prepared in more acidic conditions [25]. Capsule stiffness is characterized by the 2D elastic shear modulus of the membrane G_s.

2.2. Microfluidic device

The sorting device (Fig. 1) consists of a straight rectangular channel of width w and depth h that contains a semi-cylindrical obstacle of diameter λ at its end (Fig. 1c). Upstream of the main channel, a flow-focusing module is added to focus the capsules onto the center of the obstacle (Fig. 1). Downstream of the obstacle, the channel widens (Fig. 1a), then splits into several exits. The width of the confined zone between the side wall and the obstacle was chosen to be smaller than the capsule size (Fig. 1d). We define as δ the distance between the center of mass of the capsule and the pillar.

2.3. Production of the microfluidic device

Microfluidic chips are produced in PDMS using standard soft lithography techniques [32]. PDMS and curing agent (Sylgard) are mixed in a 10:1 ratio and cast onto the master, which consists of a silicon wafer with SU8-photoresist microstructures (Microfactory, Paris). After baking for 2 h at 70 °C, the PDMS is cross-linked and can be peeled off from the SU8 master. It is then plasma-bounded together with a glass slide using air plasma generated by a plasma-oxidizer (HARRICK, NY 14850, USA). After 2 h in a stove at 70 °C, the device is ready to be used.

2.4. Experimental setup

The sketch of our experimental setup is shown in Fig. 1. A pressure controller (MFCS, Fluigent, France) is used to impose a pressure P_{in} to the core fluid and a pressure P_{ext} to the external fluid. The chip is placed on the stage of an inverted microscope (DMIL LED, Leica Microsystems GmbH, Germany). Videos are recorded using a high-speed camera (Fastcam SA3, Photron, USA).

2.5. Coflow experiments

We carry out coflow experiments with miscible fluids. The reservoirs containing the external and internal fluids are connected to the pressure controller using PEEK tubes with an internal diameter of 0.25 mm. A fluid of viscosity μ_{in} is perfused at pressure P_{in} into another fluid of viscosity μ_{ext} moved at pressure P_{ext} ($\mu_{in} < \mu_{ext}$). The pressures applied to each entrance are adjusted, varying P_{in}/P_{ext} in order to control the core flow width ϵ

Please cite this article as: D. Vesperini et al., Deformability- and size-based microcapsule sorting, Medical Engineering and Physics (2017), http://dx.doi.org/10.1016/j.medengphy.2017.06.040

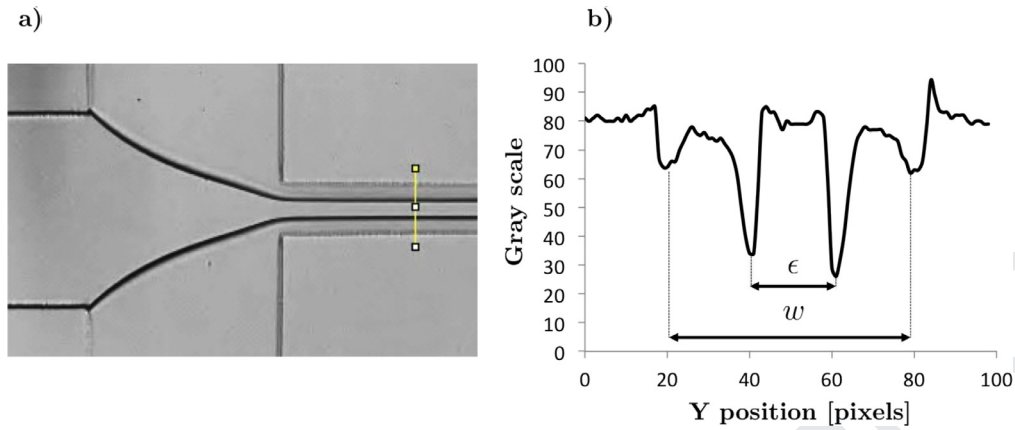

Fig. 2. (a) Photograph of a coflow of an internal flow of pure water injected into a solution of 70% of glycerol (Fluid pair A, Table 1). (b) Gray scale profile along the yellow line (Fig. 2a) used to measure the inner flow width ϵ, and the width of the channel w. (For interpretation of the references to color in this figure legend, the reader is referred to the web version of this article). Q3

Table 1
Fluid properties for different coflows with μ_{in} (resp. μ_{ext}) as the viscosity of the inner fluid (resp. external fluid), and the viscosity contrast $\chi^{-1} = \mu_{ext}/\mu_{in}$.

Fluid pair	Internal fluid	External fluid	μ_{in}[cP]	μ_{ext}[cP]	χ^{-1}
A	Pure water	Glycerol 70%	1	30	30
B	Alginate solution	Glycerol 70%	7	30	4
C	Capsule suspension	Pure glycerol	800	1300	2

(Fig. 1b). Different fluid pairs (Table 1) are used for calibrating the flow and establishing the relationship between the flow rate ratio $\phi = q_{in}/q_{ext}$ and the width ϵ.

Coflow experiments are performed with different fluids, whose properties are summarized in Table 1. We prepare a 70% glycerol/water mixture (24397-365, VWR, France) and a 1% (w/w) low viscosity alginate (A1112, Sigma-Aldrich, St Louis, MO, USA) solution in water containing 0.9% NaCl and 0.2% Hepes. The alginate solution is agitated at least 2 days at 4 °C.

For variable values of the internal and external pressures, we measure the external and internal flow rates, q_{ext} and q_{in}, in the two inlets of the flow-focusing module thanks to a flowmeter (Flowell, Fluigent, France). The value of the flow rate ratio ϕ is deduced.

Images are post-processed with the software Image J. A ROI (Region of Interest) line is drawn, containing the channel edges of the straight part (Fig. 2a). The core flow width ϵ is defined as the distance between the two minima of the gray curve plot (Fig. 2b).

2.6. Capsule flow

We prepare the capsule suspension with 20 µL of capsules in 1 g of pure glycerol. The reservoirs containing the external and internal fluids (Fluid pair C, Table 1) are connected to the pressure controller using PTFE tubes with an internal diameter of 0.3 mm. In order to accurately capture capsule trajectories in the diverging chamber, we operated at 250 frames per second with a resolution of 1024 × 768 pixels, with a 10 × magnification for all the videos and images. We measure the capsule speed U in the straight channel upstream of the obstacle, before any deformation, and the trajectory followed by the capsule in the divergent chamber (Fig. 4a), at different flow strengths. We define the flow strength as the product $\mu_{ext}U$. Varying the pressures P_{in} and P_{ext} modifies U, and in consequence the flow strength.

The position Y_c of the center of mass upstream of the obstacle is compared to the position of the middle of the channel $Y_0 = 0$. The off-centering κ is defined as the difference between the two values and non-dimensionalized by the capsule diameter D, $\kappa = \frac{Y_c - Y_0}{D}$.

3. Results

3.1. Coflow at the channel entrance

Before flowing microcapsules in our device, we flowed two miscible viscous fluids to characterize the coflow in the flow-focusing module. The aim of the flow-focusing module is to center the core flow in the straight rectangular channel upstream of the obstacle. In the experiments presented in the following section, we flow capsules in the core flow and expect them to be centered onto the obstacle. But, beforehand, we carry out coflow experiments without microcapsules to understand the coflow behavior when varying the viscosity ratio $\chi = \mu_{in}/\mu_{ext}$ (Table 1).

For a given fluid pair, the viscosity ratio is fixed Table 1), and only the inlet pressures are modified. We modify the internal pressure P_{in} keeping the external pressure P_{ext} constant, adjusting the range of variation to avoid backward surge in one or the other inlet and measure the width ϵ. We worked at variable P_{in}/P_{ext} in order to characterize the behavior of coflows and determine the relation between the width ϵ, the viscosity and flow rate ratios χ and ϕ (Fig. 3a).

The values of the internal thread width ϵ are plotted in Fig. 3 as a function of the viscosity ratio ϕ and flow rate ratio χ. It is non-dimensionalized by three different lengths α: the rectangular microchannel width w, height h and characteristic length $\sqrt{hw}$. The experimental results are plotted along with the ones published by Hu and Cubaud [33]. In their study conducted in a square cross-section channel ($w = h = \alpha$), they showed that the core thread width scales as:

$$\frac{\epsilon}{\alpha} = [1 + (1.5\chi^{1/2}\phi^{2/3})^{-1}]^{-1}. \quad (1)$$

We prove that the depth h, which is the smallest length in our device, does not limit the core flow width ϵ. In a square channel the three characteristic lengths are equal, and it was not obvious to know which characteristic length constrained the width ϵ. When ϵ is rescaled by $\alpha = \sqrt{hw}$, the data collapse onto the master curve defined by Eq. (1) (Fig. 3a). We then plot $\epsilon/\sqrt{hw}$ as a function of the flow rate ratio ϕ for different viscosity ratios χ and show that our experimental values agree with Hu and Cubaud [33] predictions (Fig. 3b). $\epsilon/\sqrt{hw}$ increases when the viscosity ratio χ^{-1} decreases. That means that the width ϵ can be easily deduced when we vary the pressures and flow strengths in the case when the

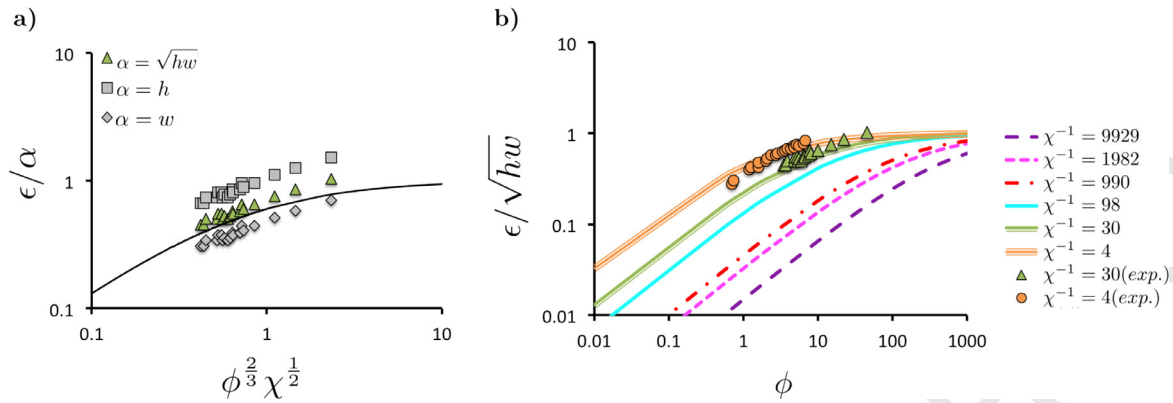

Fig. 3. The width ϵ of the core flow is expressed as a function of the flow rate ratio ϕ and the viscosity ratio χ. (a) Plot of ϵ/α for the different dimension parameters α, for the fluid pair A. Solid line represents $\epsilon/\alpha = [1 + (1.5\chi^{1/2}\phi^{2/3})^{-1}]^{-1}$. Best fit for $\alpha = \sqrt{hw}$. (b) Plot of $\epsilon/\sqrt{hw}$ as a function of ϕ for the fluid pairs A and B. Green triangles correspond to fluid pair A (water/70% glycerol mixture, $\chi^{-1} = 30$) and orange circles represent experimental data from fluid pair B (alginate/70% glycerol mixture, $\chi^{-1} = 4.28$). Solid lines represent $\epsilon/\alpha = [1 + (K_x\phi^{2/3})^{-1}]^{-1}$ ($K_x = 1.5\chi^{1/2}$) and are adapted from [33]. (For interpretation of the references to color in this figure legend, the reader is referred to the web version of this article). .

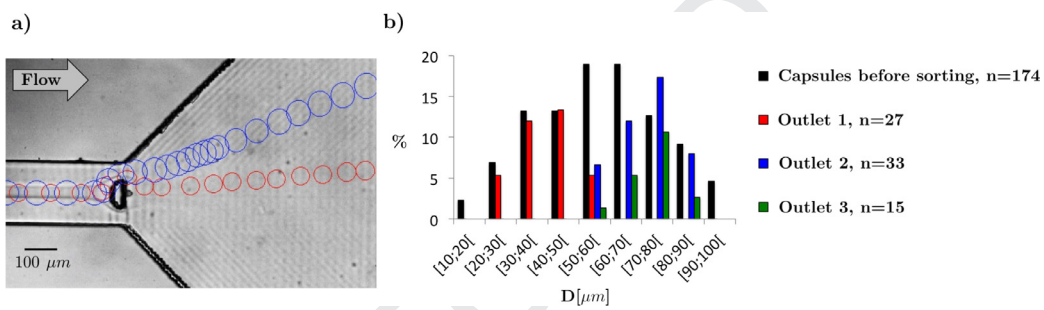

Fig. 4. (a) Trajectories of a 60 µm capsule (red) and a 80 µm capsule (blue), at various instants of time when they flow in pure glycerol (Fluid pair C, Table 1). (b) Size distribution of capsules collected at the different outlets. (For interpretation of the references to color in this figure legend, the reader is referred to the web version of this article).

optical contrast between the 2 fluids is low or absent. In the following experiments with capsules, we apply pressures in order to have values of the internal thread size ϵ smaller than the capsule diameter D.

3.2. Influence of size on the capsule trajectory

Prior to any flow perfusion experiment, we observe capsules on a glass slide with an inverted microscope. We measure the mean diameter in statics, between slide and cover, on 174 capsules and found $D_0 = 60 \pm 18$ µm. Capsules are then flowed through a 50 µm gap between the wall and the obstacle, where they are confined. They are then collected at the different outlets Fig. 1a) and their size distribution is determined. The external fluid is pure glycerol (Fluid pair C, Table 1) with an external pressure $P_{ext} = 1000$ mbar. The internal fluid is the capsule suspension (Fluid pair C, Table 1) with an internal pressure $P_{in} = 400$ mbar.

We notice that larger capsules are deflected further from the channel axis than smaller ones (Fig. 4a). This is confirmed by the capsule size measurements at the three outlets (Fig. 4b). We found an average diameter $D_1 = 39 \pm 10$ µm for outlet 1 (in red, Fig. 1a), $D_2 = 70 \pm 8$ µm for outlet 2 (in blue, Fig. 1a) and $D_3 = 73 \pm 8$ µm for outlet 3 (in green, Fig. 1a). These results indicate that the system is able to sort micro-objects from their size. It functions as a standard pinched flow fractionation device [34]. The position of the center of mass of the capsule in the confined zone seems to influence the trajectory followed by the capsules. The smaller the capsule, the closer its center of mass from the obstacle, and the smaller δ. For an identical initial position, the larger capsules pass further from the obstacle and are more deflected than smaller ones in the divergent chamber. The trajectory of capsules seems to be sensitive to the capsule-to-obstacle distance δ, which is the only modified parameter in size-based sorting.

3.3. Influence of flow strength on the capsule trajectory

The experiment is now repeated, with the same fluids (Fluid pair C, Table 1), for different pressures: $P_{in} = 200$ mbar and $P_{ext} = 1000$ mbar (low flow strength), and $P_{in} = 1200$ mbar and $P_{ext} = 4500$ mbar (high flow strength). An increase in pressure keeping the P_{in}/P_{ext} ratio constant (constant core width ϵ) induces an increase in the flow rates q_{in} and q_{ext} and consequently in the capsule speed and forces applied to the capsule when it reaches the obstacle. Depending on the capsule mechanical properties, the capsule deforms more around the obstacle and its trajectory may vary. The capsules produced at pH 5.9 are softer than those produced at pH 8 (Table 2) [25]. We can notice that the stiffness of the two batches of capsules, defined as the ratio of G_s, differs only by a factor of 3 ± 1.5. Nonetheless, at constant flow strength, the viscous forces push softer capsules further towards the obstacle wall as they flow around it, rather than stiffer capsules. This is due to the fact that viscous forces are balanced with elastic forces and that the more the capsule deforms, the closer the center of mass of the capsule and the obstacle (small δ). We show in Fig. 5 that the flow strength may have an influence on the trajectory of some capsules, depending on their stiffness. Capsules prepared at pH = 5.9 are less deflected at high flow strength (yellow capsule, Fig. 5a) than at low flow strength (pink capsule, Fig. 5a). On the contrary, capsules prepared at pH = 8 follow roughly the same trajectory whatever the applied viscous force (Fig. 5b). For the stiffest

Table 2
Capsules produced with different pH are flowed under a pressure ratio P_{in}/P_{ext}. The velocity U is measured experimentally, and the surface shear modulus G_s arises from the experiments by Chu et al. [25]. The values of the capillary number Ca are calculated using Eq. (2).

Cond.	pH	P_{in} [mbar]	P_{ext} [mbar]	U [$mm.s^{-1}$]	G_s [$N.m^{-1}$]	Ca
1	5.9	267	1000	1.1 ± 0.1	0.030 ± 0.007	0.05 ± 0.01
2	5.9	1200	4500	5.0 ± 0.3	0.030 ± 0.007	0.22 ± 0.04
3	8	200	1000	0.7 ± 0.1	0.081 ± 0.026	0.01 ± 0.002
4	8	1200	4500	4.9 ± 0.6	0.081 ± 0.026	0.08 ± 0.02

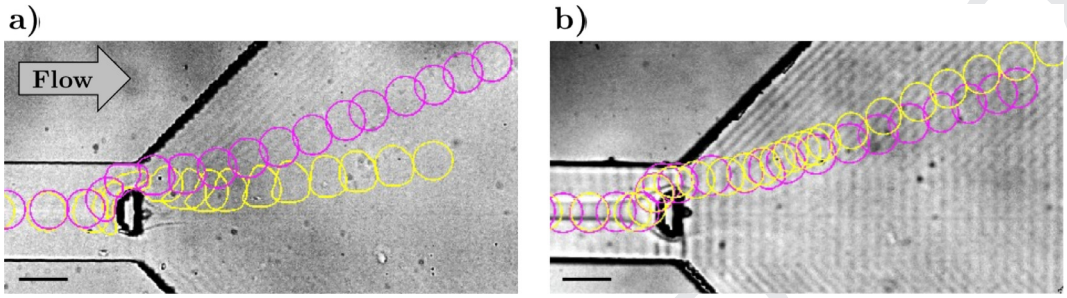

Fig. 5. Trajectory of capsules in the diverging flow chamber. Capsules were flowed at low (pink) and high (yellow) flow strengths. (a) Capsules prepared at pH 5.9. (b) Capsules prepared at pH 8. The scale bars correspond to 100 µm. (For interpretation of the references to color in this figure legend, the reader is referred to the web version of this article).

capsules (pH = 8), the trajectory is not affected by an increase in flow rates. This means that even at high pressure, the flow strength $\mu_{ext}U$ remains too small to overcome the elastic forces characterized by the 2D elastic shear modulus G_s.

4. Discussion

In the flow-focusing module at the entrance of our system, the capsule suspension forms a jet surrounded by a more viscous glycerol. The results presented in this paper show that we are able to control the width ϵ of the core flow, for a given viscosity ratio χ, by modifying the pressures applied at the entrances of our system. In the literature, the flow through flow-focusing microsystems has been abundantly studied but involves mostly the coflow of immiscible fluids, mainly for bubble [35] and droplet formation [36]. The velocity profile in the coflowing fluids differs significantly depending on whether the most viscous fluid is the internal [37] or the external one [33]. Although there are considerably fewer studies in the literature on the latter case, recent works have explored the geometry of fluid jets [33]. But no study had been conducted in rectangular channels. We show that the universal equation $\epsilon/\alpha = [1 + (1.5\chi^{1/2}\phi^{3/2})^{-1}]^{-1}$ established by Hu and Cubaud [33] in a rigid square channel for a viscosity ratio χ^{-1} between 100 and 10,000 remains valid for smaller viscosity contrasts ($\chi^{-1} = 30$ and $\chi^{-1} = 4$ in our experiments). More interestingly, the current results extend this law to soft PDMS channels with rectangular cross-section, provided the effective length scale $\alpha = \sqrt{hw}$ is used. We can imagine that for a rectangle with a larger w/h ratio, the length h would limit more effectively the width ϵ and modify the previous equation. It would be interesting to perform experiments in wider channels in order to find the limit of validity of this scaling law.

By flowing microcapsules of various sizes and mechanical properties in our device, we showed that a heterogeneous population of capsules can be sorted by size, at low flow strength. The sorting principle is similar to Pinch Flow Fractionation (PFF). In PFF systems, particles or bubbles are squeezed against a wall by an external flow. Small and large micro-objects take up distinct streamlines that can be later separated in a diverging chamber [34,38]. Unlike systems described in the literature, our device has a symmetrical design, with a constriction on each side of the obstacle. The streamline towards which smaller objects are pushed is the centerline of the channel thus it is not located along a wall. This could allow a faster collection of small objects.

As in PFF devices, the trajectory of a capsule in the sorting device is governed by the distance δ between the obstacle and the center of mass of the capsule in the confined zone. At low flow strength, δ only depends on the size of particles to be sorted and increases with capsule diameter. Viscous forces are too small to deform capsules as they flow around the obstacle. Whatever their stiffness, δ is the capsule radius ($D/2$) and δ is maximal for capsules whose diameter is equal to the constriction width. At larger flow strength $\mu_{ext}U$, hydrodynamic forces increase and become comparable to elastic forces. In this case, the distance δ between a capsule and the obstacle no longer depends solely on capsule size, but also on capsule stiffness. Capsule sorting then depends on the capillary number:

$$Ca = \frac{\mu_{ext}U}{G_s}. \quad (2)$$

The capillary number compares viscous and elastic forces. Deformable capsules are pushed closer towards the obstacle wall (low δ) and end up following the same streamline as smaller objects. We can therefore imagine sorting microcapsules by deformability using our device. This has to be done at high capillary number Ca.

For fixed G_s, capsule deformation will only occur at large capillary number, i.e. at high flow strength $\mu_{ext}U$. We seek to determine the critical capillary number Ca_c beyond which capsule trajectory starts to depend on the mechanical properties. In earlier experiments, the 2D shear modulus G_s has been measured for several conditions of pH and reticulation time [25]. At low flow strength, pH 5.9 and 8 capsules follow the same streamline: no deformability-based sorting occurs. At high flow strength, on the other hand, soft capsules deform around the obstacle while stiff capsules do not. Using Eq. (2), we find $Ca < 0.1$ for stiff capsules and/or low flow strength (Table 2). For soft capsules, at high flow strength we find $Ca > 0.2$. This yields two different values for the distance δ between the obstacle wall and the capsule center of mass, and the two populations can be separated. Our experimental results suggest that Ca_c lies between 0.1 and 0.2. This is consistent with the numerical results found in the literature, which report on a stiff behavior at $Ca = 0.05$ and soft behavior at $Ca = 0.3$

Please cite this article as: D. Vesperini et al., Deformability- and size-based microcapsule sorting, Medical Engineering and Physics (2017), http://dx.doi.org/10.1016/j.medengphy.2017.06.040

[30]. In conclusion, a moderate increase in the 2D shear modulus G_s results in a significant modification of the trajectory when we impose high pressures in order to have $Ca < 0.1$ for a population of capsules and $Ca > 0.2$ for the other one.

The populations of rigid and soft capsules used in our experiments are polydisperse, with diameters between 55 µm and 85 µm. Many size-based separation techniques require a large size contrast between objects to be sorted, and a frankly bimodal distribution [18,34]. It is quite the opposite here: when microbeads much smaller than capsules are added to the suspension, not all of them are collected in the central outlet. This is due to the fact that they are not properly centered by the flow focusing. The distance $Y_c - Y_0$ between their center of mass and the channel axis can be as large as $\epsilon - D$. Small objects are therefore much more likely to be off-centered than objects of size $D \simeq \epsilon$, which are more efficiently confined in the jet. Similarly, capsules that are much larger than the constriction have to deform to pass through the obstacle. Whatever the flow strength, they take up the whole space available and $\delta = \frac{w-\lambda}{4}$. In our system, optimal separation is thus achieved with narrow size distributions, when all objects to be sorted have a size comparable to that of the fluid thread generated by the flow focusing. In the literature, techniques based on deterministic lateral displacement or inertia have demonstrated their ability to sort bimodal populations of micro-objects. Devices relying on inertial forces to separate particles usually operate at Reynolds number (Re) between 1 and 50 [14]. In our system Re computed with particle velocity and the smallest of the 2 viscosities always remain smaller than 10^{-3}, indicating that inertial forces are negligible. We propose in this article a more sensitive device, which can sort micro-objects exhibiting moderate variability in size or deformability.

5. Conclusion

We have demonstrated that capsule sorting based on deformability and size can be achieved experimentally by using the same device at various flow rates. The present device allows us to separate and collect capsules at different outlets after sorting. It is based on the capsule ability to deform around an obstacle and to follow different trajectories depending on capsule size and stiffness. Rigid capsules follow the same trajectory, whatever the flow strength, while soft capsules are pushed towards the channel axis when the viscous forces increase.The trajectory followed by a capsule in the diffusing chamber is governed by the distance δ between the center of mass of the capsule and the obstacle in the constriction. In a polydisperse suspension, where both size and mechanical properties vary, the system can be used in two steps. A deformability-based sorting at high flow rate can follow a previous size-based separation at low flow rate, in the desired size range. This is the proof that we have developed a versatile multipurpose sorting microsystem based on a really simple design. Compared to other existing sorting devices, we demonstrate the sensitivity of our device to sort micro-objects with small size and stiffness contrasts. Further developments are expected to minimize our device dimensions and will open new perspectives to sort heterogeneous populations of cells, and help cancer diagnosis or cell differentiation.

6. Author contributions

A.L.G. conceived the experiments; D.V., O.C., P.M. and N.M. performed experiments; F.E.-L. made the capsules; D.V., A.-V.S. and A.L.G. analyzed the data; D.V., A.-V.S. and A.L.G. wrote the paper.

7. Conflict of interests

The authors declare no conflict of interests. The founding sponsors had no role in the design of the study, in the collection, analyses, or interpretation of data, in the writing of the manuscript, or in the decision to publish the results.

Acknowledgments

D.V. acknowledges financial support from the French Ministry of Research. This project has been funded by Picardy Region (FORPLAQ project). Q4

References

[1] Zhao H, Shaqfeh ES, Narsimhan V. Shear-induced particle migration and margination in a cellular suspension. Phys Fluids 2012;24:011902. doi:10.1063/1.3677935.
[2] Dong C, Lei XX. Biomechanics of cell rolling: shear flow, cell-surface adhesion, and cell deformability. J Biomech 2000;33:35–43. doi:10.1016/S0021-9290(99)00174-8.
[3] Woodward J. Crossing the endothelium. Cell Adhes Migr 2008;2:151–2.
[4] Condeelis J, Segall JE. Intravital imaging of cell movement in tumours. Nat Rev Cancer 2003;3:921–30. doi:10.1038/nrc1231.
[5] Mills JP, Diez-Silva M, Quinn DJ, Dao M, Lang MJ, Tan KSW, et al. Effect of plasmodial RESA protein on deformability of human red blood cells harboring Plasmodium falciparum. PNAS 2007;104:9213–17. doi:10.1073/pnas.0703433104.
[6] Suresh S. Biomechanics and biophysics of cancer cells. Acta Mater 2007;55:3989–4014. doi:10.1016/j.actamat.2007.04.022.
[7] Gossett DR, Weaver WM, Mach AJ, Hur SC, Tse HTK, Lee W, et al. Label-free cell separation and sorting in microfluidic systems. Anal Bioanal Chem 2010;397:3249–67. doi:10.1007/s00216-010-3721-9.
[8] Inglis DW. Efficient microfluidic particle separation arrays. Appl Phys Lett 2009;94:013510. doi:10.1063/1.3068750.
[9] Huang LR, Cox EC, Austin RH, Sturm JC. Continuous particle separation through deterministic lateral displacement. Science 2004;304:987–90. doi:10.1126/science.1094567.
[10] Guo F, Ji X-H, Liu K, He R-X, Zhao L-B, Guo Z-X, et al. Droplet electric separator microfluidic device for cell sorting. Appl Phys Lett 2010;96:193701. doi:10.1063/1.3360812.
[11] Choi S, Song S, Choi C, Park J-K. Microfluidic self-sorting of mammalian cells to achieve cell cycle synchrony by hydrophoresis. Anal Chem 2009;81:1964–8. doi:10.1021/ac8024575.
[12] Shields CW, Johnson LM, Gao L, López GP. Elastomeric negative acoustic contrast particles for capture, acoustophoretic transport, and confinement of cells in microfluidic systems. Langmuir 2014;30:3923–7. doi:10.1021/la404677w.
[13] Petersson F, Aberg L, Sward-Nilsson A-M, Laurell T. Free flow acoustophoresis: Microfluidic-based mode of particle and cell separation. Anal Chem 2007;79:5117–23. doi:10.1021/ac070444e.
[14] Kuntaegowdanahalli SS, Bhagat AAS, Kumar G, Papautsky I. Inertial microfluidics for continuous particle separation in spiral microchannels. Lab Chip 2009;9:2973–80. doi:10.1039/b908271a.
[15] Nagrath S, Sequist LV, Maheswaran S, Bell DW, Irimia D, Ulkus L, et al. Isolation of rare circulating tumour cells in cancer patients by microchip technology. Nature 2007;450:1235–9. doi:10.1038/nature06385.
[16] Baret J-C, Miller OJ, Taly V, Ryckelynck M, El-Harrak A, Frenz L, et al. Fluorescence-activated droplet sorting (FADS): efficient microfluidic cell sorting based on enzymatic activity. Lab Chip 2009;9:1850–8. doi:10.1039/b902504a.
[17] Guck J, Ananthakrishnan R, Mahmood H, Moon TJ, Cunningham CC, Käs J. The optical stretcher: a novel laser tool to micromanipulate cells. Biophys J 2001;81:767–84. doi:10.1016/S0006-3495(01)75740-2.
[18] Wang G, Mao W, Byler R, Patel K, Henegar C, Alexeev A, et al. Stiffness dependent separation of cells in a microfluidic device. Plos One 2013;8:e75901. doi:10.1371/journal.pone.0075901.
[19] Shields CW, Reyes CD, López GP. Microfluidic cell sorting: a review of the advances in the separation of cells from debulking to rare cell isolation. Lab Chip 2015;15:1230–49. doi:10.1039/c4lc01246a.
[20] Gossett DR, Tse HTK, Lee SA, Ying Y, Lindgren AG, Yang OO, et al. Hydrodynamic stretching of single cells for large population mechanical phenotyping. PNAS 2012;109:7630–5. doi:10.1073/pnas.1200107109.
[21] Walter J, Salsac A-V, Barthès-Biesel D, Le Tallec P. Coupling of finite element and boundary integral methods for a capsule in a Stokes flow. Int J Numer Methods Eng 2010;83:829–50. doi:10.1002/nme.2859.
[22] Kaoui B, Krüger T, Harting J. Complex dynamics of a bilamellar vesicle as a simple model for leukocytes. Soft Matter 2013;9:8057–61. doi:10.1039/c3sm51032h.
[23] Dupin MM, Halliday I, Care CM, Alboul L, Munn LL. Modeling the flow of dense suspensions of deformable particles in three dimensions. Phys Rev E 2007;75:066707. doi:10.1103/PhysRevE.75.066707.
[24] Gubspun J, Gires P-Y, de Loubens C, Barthès-Biesel D, Deschamps J, Georgelin M, et al. Characterization of the mechanical properties of cross-

linked serum albumin microcapsules: effect of size and protein concentration. Colloid Polym Sci 2016;294:1381–9. doi:10.1007/s00396-016-3885-8.

[25] Chu TX, Salsac A-V, Leclerc E, Barthès-Biesel D, Wurtz H, Edwards-Lévy F. Comparison between measurements of elasticity and free amino group content of ovalbumin microcapsule membranes: discrimination of the cross-linking degree. J Colloid Interface Sci 2011;355:81–8. doi:10.1016/j.jcis.2010.11.038.

[26] Dawson G, Häner E, Juel A. Extreme deformation of capsules and bubbles flowing through a localised constriction. Proc IUTAM 2015;16:22–32. doi:10.1016/j.piutam.2015.03.004.

[27] De Cock LJ, De Koker S, De Geest BG, Grooten J, Vervaet C, Remon JP, et al. Polymeric multilayer capsules in drug delivery. Angew Chem 2010;49:6954–73. doi:10.1002/anie.200906266.

[28] Leclerc E, Kinoshita H, Fujii T, Barthès-Biesel D. Transient flow of microcapsules through convergent–divergent microchannels. Microfluid Nanofluid 2012;12:761–70. doi:10.1007/s10404-011-0907-1.

[29] Gires P-Y, Barthès-Biesel D, Leclerc E, Salsac A-V. Transient behavior and relaxation of microcapsules with a cross-linked human serum albumin membrane. J Mech Behav Biomed Mater 2016;58:2–10. doi:10.1016/j.jmbbm.2015.09.008.

[30] Zhu L, Rorai C, Mitra D, Brand L. A microfluidic device to sort capsules by deformability: a numerical study. Soft Matter 2014;10:7705–11. doi:10.1039/C4SM01097C.

[31] Edwards-Lévy F, Andry M-C, Lévy M-C. Determination of free amino group content of serum albumin microcapsules using trinitrobenzenesulfonic acid: effect of variations in polycondensation pH. Int J Pharmaceut 1993;96:85–90. doi:10.1016/0378-5173(93)90215-2.

[32] Whitesides GM, Ostuni E, Takayama S, Jiang X, Ingber DE. Soft lithography in biology and biochemistry. Annu Rev Biomed Eng 2001;3:335–73. doi:10.1146/annurev.bioeng.3.1.335.

[33] Hu X, Cubaud T. Inertial destabilization of highly viscous microfluidic stratifications. Phys Rev Fluids 2016;1:044101. doi:10.1103/PhysRevFluids.1.044101.

[34] Yamada M, Nakashima M, Seki M. Pinched flow fractionation: continuous size separation of particles utilizing a laminar flow profile in a pinched microchannel. Anal Chem 2004;76:5465–71. doi:10.1021/ac049863r.

[35] Nie Z, Seo M, Xu S, Lewis PC, Mok M, Kumacheva E, et al. Emulsification in a microfluidic flow-focusing device: effect of the viscosities of the liquids. Microfluid Nanofluid 2008;5:585–94. doi:10.1007/s10404-008-0271-y.

[36] Garstecki P, Fuerstman MJ, Stone HA, Whitesides GM. Formation of droplets and bubbles in a microfluidic T-junction-scaling and mechanism of break-up. Lab Chip 2006;6:437–46. doi:10.1039/b510841a.

[37] Cubaud T, Masson TG. Capillary threads and viscous droplets in square microchannels. Phys Fluids 2008;20:053302. doi:10.1063/1.2911716.

[38] Maenaka H, Yamada M, Yasuda M, Seki M. Continuous and size-dependent sorting of emulsion droplets using hydrodynamics in pinched microchannels. Langmuir 2008;24:4405–10. doi:10.1021/la703581j.

Please cite this article as: D. Vesperini et al., Deformability- and size-based microcapsule sorting, Medical Engineering and Physics (2017), http://dx.doi.org/10.1016/j.medengphy.2017.06.040